Numerical and Physical Experiments of Wave Focusing in Short-Crested Seas

Félicien Bonnefoy, Pierre Roux de Reilhac, David Le Touzé & Pierre Ferrant

Équipe Hydrodynamique et Génie Océanique
École Centrale de Nantes
B.P. 92101, F-44321 Nantes, France
pierre.ferrant@ec-nantes.fr

Abstract. This paper aims at determining the wave generator motion required to deterministically reproduce a prescribed wave packet in a wave basin. In two dimensions, a partial model at third order is proposed, which accounts for the nonlinear phase velocities during the propagation from the wavemaker to the focusing point. Advantage is being taken of knowing these nonlinear velocities to build a command law of the wave generator that notably enhances the quality of the target reproduction, both in numerics and in experiments. In three dimensions where directionality adds significant complexity to the reproduction process, a linear decomposition of the target wave packet is developed, one frequency per direction, starting from a set of five wave probe measurements.

Introduction

The evolution of extreme waves due to the focusing of several wave components is studied both in laboratory experiments and simulation. Our main concern here is to deterministically reproduce in a wave basin a large wave event that could have been measured in the open ocean or in our case generated preliminary in the wave basin. The unknown is the wavemaker motion.

Whereas the classical use of linear backward propagation and transfer function of the wavemaker leads to good results in small amplitude waves, this approach obviously fails at larger amplitudes and hence needs further improvement. The estimation of the nonlinear phase velocity is the key point for accurate reproduction of deterministic wave trains, see *e.g.* the iterative technique of Clauss *et al.* [4]. In two dimensions, the direct iterative corrections of the wavemaker motion frequency components [3] have furnished a first attempt to improve the reproduction both for experiments and numerical simulations using a fast and accurate fully nonlinear spectral model [8, 2]. This original model reproduces the complete 3D wave basin with perfectly reflecting sidewalls, damping at one end to simulate the physical beach and generation process by imposing an inlet flux condition on the opposite boundary of the domain. A novel approach is considered here where the nonlinear phase speed is evaluated from the generation of the wave packets with the determined input (crest focusing η) and the π radians out of phase input (trough focusing η_π). The correction of the wavemaker motion

with this adjusted phase velocity shows considerable improvement of the reproduced wave field. In three dimensions, arrays of probes are generally too coarse to produce reliable results from a spatial Fourier Transform so an alternative approach is investigated to deduce the wavemaker motion.

1 Wave basins

The methods of deterministic reproduction studied here have been tested in both numerical and physical basins that we briefly describe in the following sections.

1.1 Fully nonlinear numerical model

We consider a three-dimensional wave tank of length L_x, width L_y and constant water depth h, filled with water assumed to be an inviscid fluid (see Fig. 1). Under

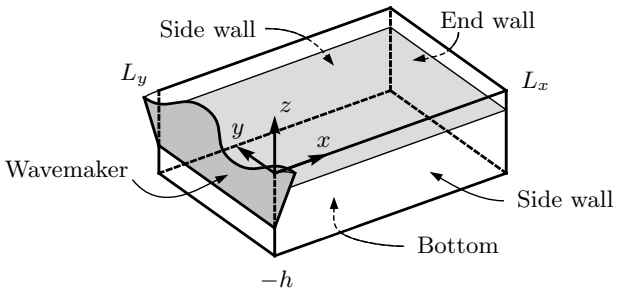

Fig. 1. Sketch of the wave basin

the potential-flow theory assumption, the unknown velocity potential $\phi(\mathbf{x}, z, t)$ satisfies Laplace's equation in the whole fluid domain D. Side and end walls are reflecting waves perfectly, and are modeled by no-flux conditions $\partial\phi/\partial n = 0$. The wave generation is taken into account on the wavemaker boundary through a linear flux condition $\partial\phi/\partial x = \partial X/\partial t$ on $x = 0$ where $X(y, z, t)$ is the wavemaker motion [2]. An additional potential ϕ_a (Agnon and Bingham [1]) is introduced by separating the potential in two $\phi = \phi_w + \phi_a$. The additional potential satisfies Laplace equation in the domain, homogeneous Neumann conditions on the walls, no condition on the free surface and the flux condition on $x = 0$. It is solved in an extended basin, in the time domain to deal with elaborated wavemaker motion $X = G(z)F(y, t)$ with G the vertical geometry (flap or piston) and F the control law to generate oblique waves. The second potential ϕ_w needs to satisfy the Laplace equation, the free surface boundary conditions (FSBCs) and homogeneous Neumann conditions on the walls, including the wavemaker $x = 0$.

The free surface potential $\phi^s(\mathbf{x},t) = \phi_w(\mathbf{x}, z=\eta, t)$ is introduced and the fully nonlinear FSBCs are rewritten as follows

$$\frac{\partial \eta}{\partial t} = \left(1+|\boldsymbol{\nabla}\eta|^2\right) W + \frac{\partial \phi^{add}}{\partial z} - \boldsymbol{\nabla}\left(\phi^s + \phi_a\right).\boldsymbol{\nabla}\eta \qquad \text{for} \quad z=\eta, \tag{1a}$$

$$\frac{\partial \phi^s}{\partial t} = -g\,\eta - \frac{1}{2}|\boldsymbol{\nabla}\phi^s|^2 + \frac{1}{2}\left(1+|\boldsymbol{\nabla}\eta|^2\right) W^2 - \nu\frac{\partial \eta}{\partial t} - \boldsymbol{\nabla}\phi^s.\boldsymbol{\nabla}\phi_a - \frac{\partial \phi_a}{\partial t} - \frac{1}{2}|\widetilde{\boldsymbol{\nabla}}\phi_a|^2 \qquad \text{for} \quad z=\eta, \tag{1b}$$

with $W = \frac{\partial \phi_w}{\partial z}(\mathbf{x}, z=\eta, t)$. Here the additional potential acts in the form of forcing terms on the RHS of the FSBCs. The damping pressure $-\nu\frac{\partial \eta}{\partial t}$ added on the dynamic FSBC (1b) provides an efficient model for the absorbing beach at the opposite of the basin, the coefficient $\nu(\mathbf{x})$ being non-zero only in a region close to the end wall (no term is added in the kinematic FSBC (1a) to ensure mass conservation). The High-Order Spectral approach (HOS) of Dommermuth and Yue [5] is used to approximate the vertical velocity W through a double series expansion (Taylor series around $z=0$ and powers of η). To obtain a consistent development in powers of η in the two terms $\left(1+|\boldsymbol{\nabla}\eta|^2\right) W$ and $\left(1+|\boldsymbol{\nabla}\eta|^2\right) W^2$ of Eqn. (1), we adopt the formulation of West *et al.* [11] for these terms.

Both the additional and the wave potential are solved with a spectral method combined with adequate dealiasing procedures, thus providing fast and accurate computations.

1.2 Physical model

In parallel to the numerical simulations presented above, wave experiments are conducted in the 50 x 30 x 5 m wave basin in ECN. The segmented wavemaker consists of 48 paddles (0.6 m width, hinged at mid depth), allowing directional wave generation. Wave elevations are measured at several locations with 1 m resistive wave probes.

The wavemaker is controlled in the frequency domain by a set of wave components (frequency, amplitude, phase plus angle in 3D wave fields). The motion is deduced by applying the linear transfer function of the wavemaker. The same frequency components are used to derive the numerical flux at the wavemaker wall with the same transfer function so that the two generation processes correspond. Dalrymple's method is used for directional wave fields to take advantage of the reflective side walls and correctly generate the large wave angles.

1.3 Comparisons

Comparisons were carried out between the numerical and physical wave basins to validate our numerical approach. Simulations of regular waves show the ability of the numerical model to reproduce the effects of high order nonlinearities such as the increase of the wave velocity due to finite amplitude and the presence of return current in the basin (not shown here for brevity, see [8, 2]). The case

of long time irregular wave fields has been investigated. Figure 2 presents an example of 900 s long 2D experiment of a modified two parameters Pierson-Moskowitz spectrum (H_s = 16 cm and T_Z = 1.4 s, that is a characteristic steepness $\varepsilon_c = H_s/\lambda_p$ = 3 % with λ_p the wavelength at the peak frequency). The time window in Fig. 2 isolates a large wave event at t = 488 s among the 640 generated waves and shows a very good agreement between the experimental data and the fully nonlinear model (HOS). For comparison, results obtained from a second order model [9] previously developed are also plotted in Fig. 2 and show inadequacy of second order theory to accurately model the large event.

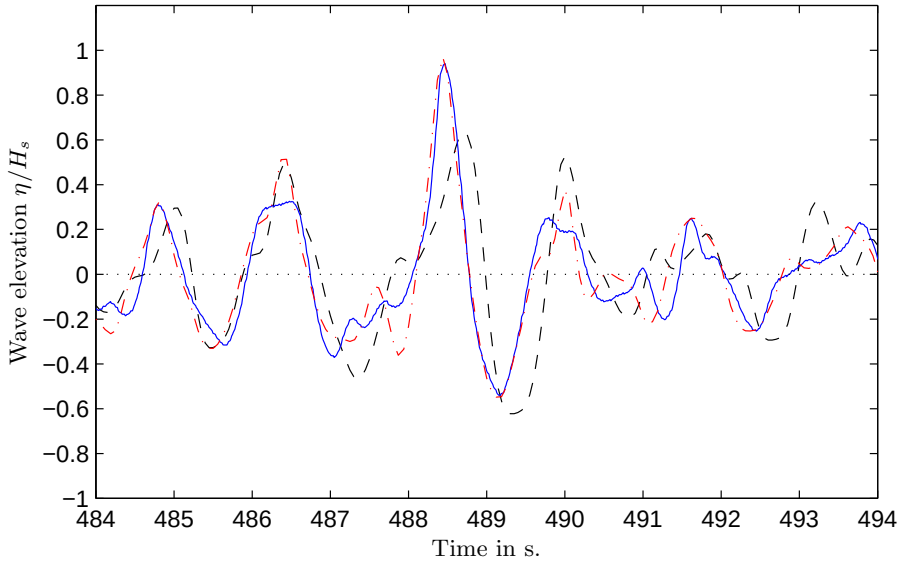

Fig. 2. Wave elevation: experimental (—), second order simulation (**--**) and HOS simulation (- · -)

The more specific case of a focused wave packet is shown in Fig. 3 (40 cm amplitude and peak wavelength λ_p=9 m). The fully nonlinear model compares satisfactorily to the experiments. Especially phases are correctly solved so the main peak is well described. In the following, we use alternatively the numerical or the physical experiments.

2 Deterministic reproduction in two dimensions

2.1 Principle

Basic linear and second order decompositions (see appendices A and B) yield satisfactory results only when the packet steepness is small. Their application to higher steepness reveals differences between the wave packet generated from

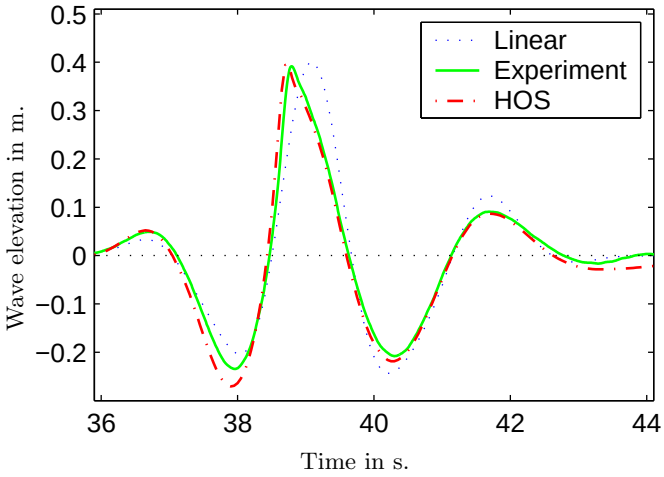

Fig. 3. Comparisons between experimental and numerical elevations

the linear or second order decomposition input and the target event. Those differences are believed here to be due mainly to the nonlinear increase of phase velocity by four wave resonant interactions as predicted in [10]. Iterative corrections of the wavemaker motion [3] show improvement for frequencies around the peak of the spectrum whereas uncorrect control of the high frequency range is observed. We thus developed a two-steps method to directly estimate the modification of the phase velocity due to nonlinear interactions. The first step is the double generation of the wave packet, one with amplitudes determined by a simple decomposition technique either linear or second order (crest focusing) and one with 180° out of phase amplitudes (trough focusing). The second step is the even/odd decomposition of the nonlinear effects (*e.g.* [7]):

$$\eta_{even} = (\eta + \eta_\pi)/2, \tag{2a}$$

$$\eta_{odd} = (\eta - \eta_\pi)/2 \ . \tag{2b}$$

2.2 Validation

This decomposition is first validated with a low amplitude wave packet in which the nonlinear effects are reduced to second order. Figure 4 (left) shows a very good agreement between the odd elevation given by Eqn. (2b) and the linear theoretical elevation calculated from the wavemaker frequency components. On the same figure (right), the even elevation given by Eqn. (2a) is correctly modeled by a second order elevation build with an expression similar to (6).

For larger wave steepness, the odd surface elevation is interpreted as the superposition of components with the linear input amplitudes and phases but modified phase velocity (or wavenumbers k'_n):

$$\eta_{odd} \quad \simeq \quad \sum_n \underline{a_n} \, e^{i(\omega_n t - k'_n x)} \ . \tag{3}$$

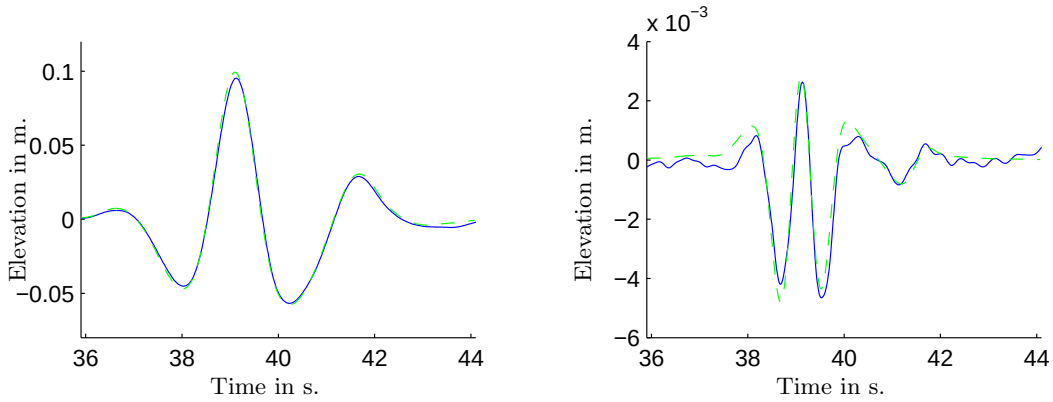

Fig. 4. Odd/even decompositions and analytical solutions (amplitude A=10 cm: left η_{odd} (—), linear (- · -), right η_{even} (—) and second order (- · -))

After a Fourier Transform of the odd elevation, the modified wavenumber k'_n is determined from Eqn. (3) and from the complex amplitude $\underline{a_n}$ known from a linear or second order theory. This provides a simple evaluation of the nonlinear phase velocity. Figure 5 (left) shows a comparison between the measured odd elevation and two linear elevations calculated from the wavemaker components either with the linear phase velocity or the estimated nonlinear phase velocity (named *corrected* in the legend). The correction of the linear elevation leads to satisfactory results as expected. A stronger validation is given at second order in Fig. 5 (right). The corrected second order elevation calculated with Eqn. (6) but with estimated nonlinear phase velocity is in good agreement with the measured even elevation, whereas the classical second order elevation (Eqn. (6)) fails to describe the even elevation.

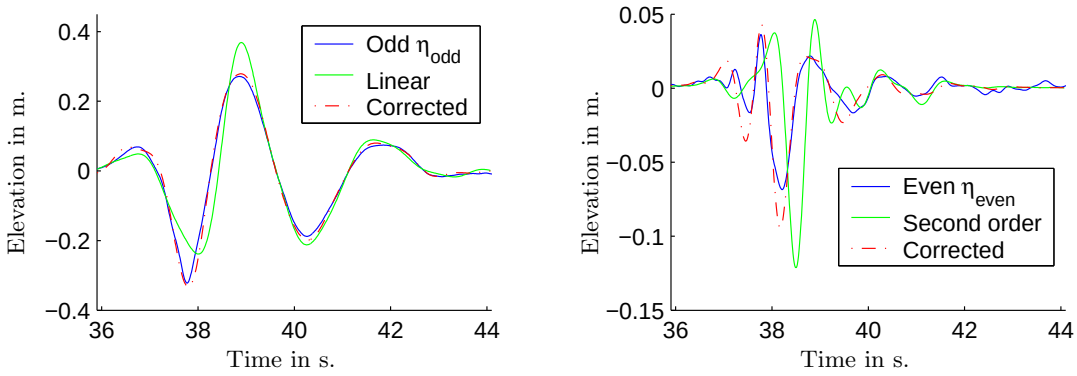

Fig. 5. Odd/even decomposition and analytical elevations with linear or nonlinear phase velocity (amplitude A=40 cm)

2.3 Application

After having evaluated the nonlinear phase velocity occurring during the focusing of the generated wave packet, we correct the wavemaker motion with the corresponding phase shift $\exp -i(k'_n - k_n)x$. Figure 6 presents the measured surface elevation at the focusing location for the reproduced wave packets, from both the initial input and the nonlinear phase velocity corrected input. Comparison with the target elevation shows the better agreement obtained with the nonlinear correction. The main features of the focused target wave packet are well reproduced with one correction of the wavemaker motion (non iteration required). The main crest and the lateral trough are close to the target in both amplitudes and phases. The main crest amplitude is correctly estimated showing a better control of the high-frequency range than in the previous iterative scheme [3].

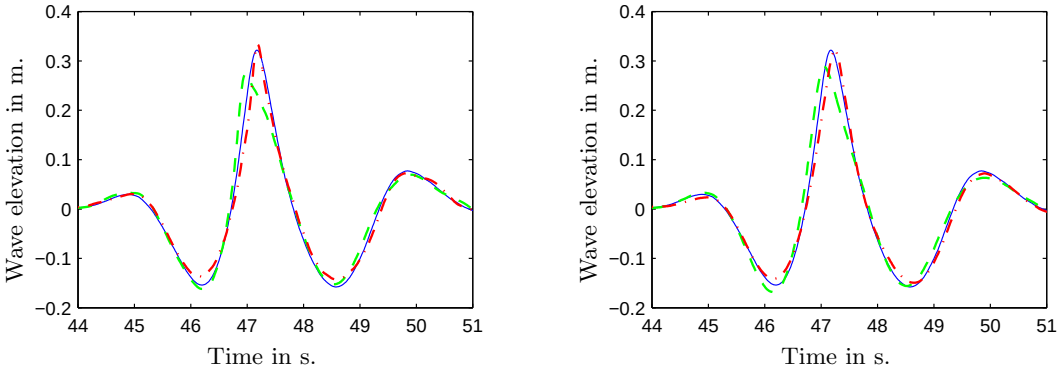

Fig. 6. Wave elevation: target (—), initial input(--) and corrected input (- · -) (left: linear input, right: second order input)

3 Deterministic reproduction in three dimensions

A first step towards directional deterministic reproduction is achieved. The target wave field is a directional wave packet, measured in a wave basin with five probes, set in a truncated pentagon shape commonly used for laboratory irregular directional wave analysis. This target is seen as the linear superimposition of directional waves, with a single direction per frequency. The Fourier Transforms of the five recorded surface elevations form the RHS of a set of nonlinear equations

$$a\, e^{-ik(x_p \cos\theta + y_p \sin\theta)+\phi} \quad = \quad TF(\eta_p) \text{ for } p = 1 \text{ to } 5, \tag{4}$$

where the unknowns are the amplitude a, the direction θ and phase ϕ. This system is solved with a nonlinear least squares method where initial guess for the

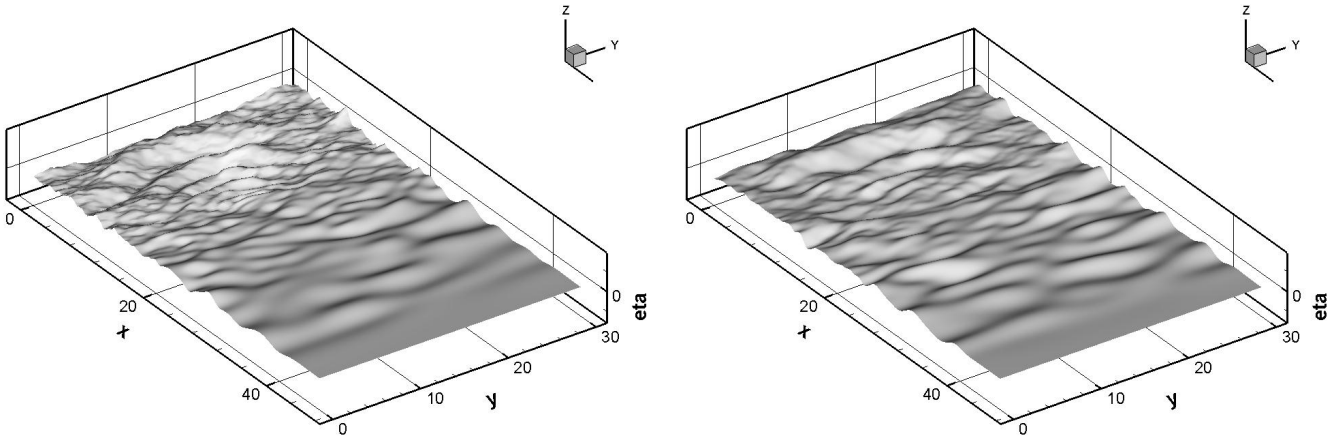

Fig. 7. View of the target wave field (left) and the reproduced one (right) at $t = 33$ s

three unknowns is provided respectively by the mean of the probe Fourier modulus, a gaussian random angle with estimated mean direction and spreading and a random phase. Local minima are expected so several solutions are computed with different initial guess and the solution is selected for the reproduction as the one that minimises the time integral squared errors between target surface height and linearly reconstructed elevation on the five probes. We finally obtain a set of directional components that is linearly propagated backwards to the wavemaker to calculate its motion. In case the requested direction of the wave is too high regarding the dimensions of the basin, the wavelength and the capabilities of the serpent-type wavemaker Dalrymple's method is used to control the motion and avoid spurious reflection on the sidewalls. Figures 7 and 8 show views of the target and reproduced wave fields at $t = 33$ s and $t = 45$ s, respectively before and at the focusing event. The main features of the focusing packet are correctly estimated by the described method although the high frequency range is underestimated. At the focusing time (Fig. 8), the reproduced wave packet is larger than the target one and its amplitude lower.

4 Conclusion

Two approaches of deterministic reproduction in 2D and 3D wave basin have been tested. The wavemaker motions are tested indifferently in the HOS fully nonlinear numerical basin or the physical basin at ECN. In 2D, the separation of odd and even nonlinear effects up to the third order leads to an estimation of the nonlinear phase velocity. Used to deduce the wavemaker motion required for the generation of a target wave packets, this nonlinear velocity yields satisfactory results for highly nonlinear targets.

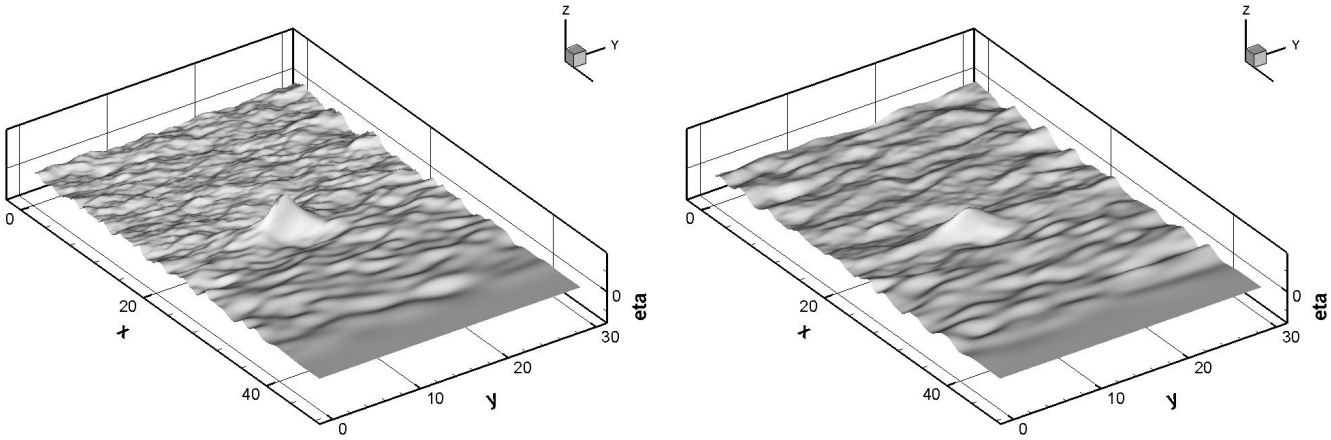

Fig. 8. View of the target wave field (left) and the reproduced one (right) at $t = 45$ s

In 3D, a basic approach is build for the reproduction of focused directional wave packets. Assuming that each frequency components has a single direction, this approach gives encouraging first results, although a better control of the high-frequency range and a study of the nonlinear effects are required.

A Appendix: Linear decomposition

In two dimensions, the wavemaker motion can be easily derived by linear theory, provided the wave packet steepness is sufficiently small. In such a case the target elevation η_c required at a distance x_c from the wavemaker is seen as the superimposition of frequency components whose complex amplitudes $\underline{c_n}$ are given by Fourier Transform of η_c.

$$\eta_c(t) \quad = \quad \sum_n \underline{c_n}\, e^{i\omega_n t} \quad = \quad \eta^{(1)}(x_c,t) \quad = \quad \sum_n \underline{\widehat{a_n}}\, e^{i(\omega_n t - k_n x_c)} \ . \qquad (5)$$

Knowing from the dispersion relation the phase speed $v_n = \omega_n/k_n$ of each component, the wave amplitudes $\underline{\widetilde{a_n}}$ at the wavemaker are simply $\underline{\widetilde{a_n}} = \underline{c_n} \exp(ik_n x_c)$. The transfer function of the wavemaker is then applied to get the required motion.

B Appendix: Second order decomposition

The iterative technique of Duncan et Drake [6] describes the target elevation as the superimposition of a linear elevation plus its bound second order elevation,

that is $\eta_c = \eta^{(1)} + \eta^{(2)}$. The linear part may be written as in (5) and the second order component as

$$\eta^{(2)} \quad = \quad \sum_{m \geq n} \underline{\widehat{a_m}}\, \underline{\widehat{a_n^{\pm}}}\, G_{mn}^{\pm}\, e^{i((\omega_m \pm \omega_n)t - (k_m \pm k_n)x)}, \tag{6}$$

with $\underline{\widehat{a_n^{+}}} = \underline{\widehat{a_n}}$ and $\underline{\widehat{a_n^{-}}}$ its conjugate. The linear amplitudes at the wavemaker location $x = 0$ are then used to build the required wavemaker motion.

References

1. Y. Agnon and H. B. Bingham. A non-periodic spectral method with applications to nonlinear water waves. *Eur. J. Mech. /B Fluids*, 18:527–534, 1999.
2. F. Bonnefoy. Modélisation expérimentale et numérique des états de mer complexes. *Ph-D Thesis*, École Centrale de Nantes, 2005.
3. F. Bonnefoy, D. Le Touzé, and P. Ferrant. Generation of fully-nonlinear prescribed wave fields using a high-order spectral method. In *Proc. ISOPE*, 2004.
4. G. F. Clauss *et al.* Non-linear calculation of tailored wave trains for experimental investigations of extreme structure behaviour. In *Proc. OMAE*, 2004.
5. D. G. Dommermuth and D. K. Yue. A high-order spectral method for the study of nonlinear gravity waves. *J. Fluid Mech.*, 184:267–288, 1987.
6. P. E. Duncan and K. R. Drake. A note on the simualtion and analysis of irregular non-linear waves. *App. Ocean Res.*, 17:1–8, 1995.
7. T. Johannessen and C. Swan. A laboratory study of the focusing of transient and directionally spread surface water waves. *Proc. R. Soc. of Lond.*, 457:971–1006, 2001.
8. D. Le Touzé. Méthodes spectrales pour la modélisation non-linéaire d'écoulements à surface libre instationnaire. *Ph-D Thesis*, École Centrale de Nantes, France, 2003.
9. D. Le Touzé, F. Bonnefoy and P. Ferrant. Second-Order Spectral Simulation of Directional Wave Generation and Propagation in a 3D Tank. In *Proc. ISOPE*, 2002.
10. M. S. Longuet-Higgins and O. M. Phillips. Phase velocity effects in tertiary wave interactions. *J. Fluid Mech.*, 12:333–336, 1962.
11. B. J. West *et al.* . A new numerical method for surface hydrodynamics. *J. Geoph. Res.*, 92(C11):11,803–11,824, 1987.